Zwitterion Functionalized Carbon Nanotube/Polyamide Nanocomposite Membranes for Water Desalination

Wai-Fong Chan,[†,∥] Hang-yan Chen,[‡,∥] Anil Surapathi,[†] Michael G. Taylor,[‡] Xiaohong Shao,[§] Eva Marand,[†,*] and J. Karl Johnson[‡,⊥,*]

[†]Department of Chemical Engineering, Virginia Polytechnic Institute and State University, 138 Randolph Hall, Blacksburg, Virginia 24061, United States, [‡]Department of Chemical & Petroleum Engineering, University of Pittsburgh, 15261 Benedum Hall, Pittsburgh, Pennsylvania 15213, United States, [§]College of Science, Beijing University of Chemical Technology, Beijing 100029, People's Republic of China, and [⊥]National Energy Technology Laboratory, Pittsburgh, Pennsylvania 15236, United States. [∥]These authors contributed equally.

ABSTRACT

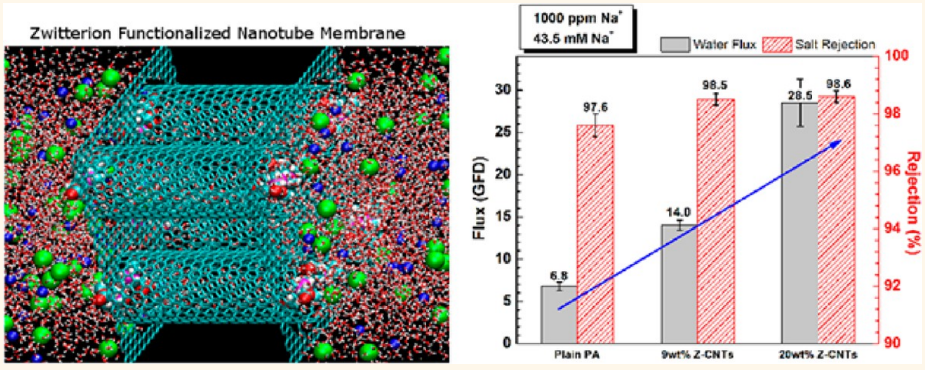

We have shown from both simulations and experiments that zwitterion functionalized carbon nanotubes (CNTs) can be used to construct highly efficient desalination membranes. Our simulations predicted that zwitterion functional groups at the ends of CNTs allow a high flux of water, while rejecting essentially all ions. We have synthesized zwitterion functionalized CNT/polyamide nanocomposite membranes with varying loadings of CNTs and assessed these membranes for water desalination. The CNTs within the polyamide layer were partially aligned through a high-vacuum filtration step during membrane synthesis. Addition of zwitterion functionalized CNTs into a polyamide membrane increased both the flux of water and the salt rejection ratio. The flux of water was found to increase by more than a factor of 4, from 6.8 to 28.7 GFD (gallons per square foot per day), as the fraction of CNTs was increased from 0 to 20 wt %. Importantly, the ion rejection ratio increased slightly from 97.6% to 98.6%. Thus, the nanotubes imparted an additional transport mechanism to the polyamide membrane, having higher flow rate and the same or slightly better selectivity. Simulations show that when two zwitterions are attached to each end of CNTs having diameters of about 15 Å, the ion rejection ratio is essentially 100%. In contrast, the rejection ratio for nonfunctionalized CNTs is about 0%, and roughly 20% for CNTs having five carboxylic acid groups per end. The increase in ion rejection for the zwitterion functionalized CNTs is due to a combination of steric hindrance from the functional groups partially blocking the tube ends and electrostatic repulsion between functional groups and ions, with steric effects dominating. Theoretical predictions indicate that an ideal CNT/polymer membrane having a loading of 20 wt % CNTs would have a maximum flux of about 20000 GFD at the conditions of our experiments.

KEYWORDS: ion rejection · reverse osmosis · molecular simulation · functionalized nanotubes

Approximately 800 million people living on the earth do not have access to safe drinking water.[1] Moreover, almost one-quarter of people on the earth live in areas where the ground water is being depleted faster than it can be replaced.[2] Although over 70% of the surface of the earth is covered with water, access to clean water remains a critical issue worldwide.[3] Clearly, finding a way to desalinate seawater, clean up brackish water, and remove harmful ions from contaminated water at low cost in a sustainable way would be a major step toward solving much of the world's water problems.

The conventional methods for desalination include distillation and reverse osmosis. The first method is unavoidably energy intensive, as water has a very high heat of

* Address correspondence to emarand@vt.edu, karlj@pitt.edu.

Received for review March 6, 2013 and accepted May 25, 2013.

Published online May 25, 2013
10.1021/nn4011494

vaporization. Reverse osmosis with semipermeable polymer membranes is an attractive option, but there is a need to improve the permeance of water, while keeping the salt rejection ratio at acceptable levels. Additionally, biofouling of RO membranes is a major problem, causing both reduced flux and high maintenance costs.[4]

Carbon nanotubes are promising materials for use in membranes because they have been shown to exhibit remarkably high flux.[5−13] Molecular simulations and experimental studies have shown that the transport of fluids through CNTs is orders of magnitude faster than through other nanoporous materials due to the unprecedented smoothness and regularity of the CNT pores.[5,8,9,11,14−17] It has been suggested that the transport of water through subnanometer CNTs occurs *via* a cooperative, pulse-like movement of hydrogen-bonded molecules within the channel, similar to what has been observed in aquaporin biological channels.[18] The transport of water in CNTs has been shown to give flow rates that are faster than predicted by classical hydrodynamics.[19,20] The enhanced water transport together with CNT pore diameters on the order of nanometers opens the possibility of employing CNTs to filter ions from water. Molecular dynamics (MD) simulation studies[21,22] have examined the ability of CNTs with diameters ranging from 0.6 to 1.1 nm to filter ions from water. These results indicated that ions can be almost completely excluded from pores up to 0.9 nm in diameter due to ion desolvation energy barriers. By contrast, water faces relatively low energy barriers and is able to pass through these small nanotubes, but at flow rates that are much lower than in larger nanotubes because water transport in these narrow CNTs is limited to single-file flow. Larger diameter CNTs have much higher water flux, but do not have the ability to reject ions. For example, Yu *et al.* also studied ion transport through CNT membranes using larger diameter (3 nm) CNTs.[23] These larger diameter nanotubes did not exhibit any ion rejection properties, but did display gated transport due to water wettability, that could be tuned by temperature, sonication, or addition of solutes.[23]

CNTs with pore diameters down to 0.4 nm have been reported,[24] so that it is at least in principle possible to produce nanotubes that would reject ions by size exclusion.[25] However, experimentally produced CNTs have a range of diameters and it is currently not possible to economically separate out nanotubes having a very narrow diameter distribution, so that producing membranes with CNTs having diameters <0.9 nm is not currently practical. An alternate approach to requiring very small diameter CNTs is to tune the effective diameter of the CNT entrance by attaching functional groups. Experimental work on ionic flux through functionalized CNTs has been reported by Hinds *et al.*[26] who showed that biotin functionalized CNTs showed a marked reduction of $Ru(NH_3)_6^+$ and by Majumder and co-workers who studied voltage gated CNT membranes formed by tethering charged molecules to the ends of large-diameter CNTs.[27] Their work has focused on studying transport of two different sized but equally charged molecules, ruthenium bipyridine and methyl viologen, through multiwalled CNTs with 7 nm nominal core diameters. They showed that flux and selectivity could be changed by applying a voltage across the membrane; this result is consistent with the charged functional groups being drawn into the CNTs at positive bias, causing a modulation of the pore size.[27] Similarly, tip and core functionalization of large diameter CNTs has been shown to modulate the flux of water, both experimentally[13] and from simulations.[28] Fornasiero *et al.* studied ion exclusion in CNTs functionalized with hydroxyl, carbonyl and carboxylic groups having pores less than 2 nm in diameter as a function of solution ionic strength, pH, and ion valence.[29,30] Their results suggest a Donnan-type rejection mechanism, dominated by electrostatic interactions between the fixed COO^- charges on the ends of the CNTs and mobile ions. However, this also means that the rejection ratios decreased significantly at higher electrolyte concentrations. The hydrated radii of the ions (∼0.6 nm) were significantly smaller than the CNT pore radius (∼1.6 nm) and therefore separation of ions by size exclusion was not possible. Atomistic simulations by Corry predicted that ion rejection can take place in CNTs having 1.1 nm diameter through the addition of functional groups having charged moieties.[31] The charged groups prevent like-charged ions from entering the tube due to electrostatic repulsion. Oppositely charged ions are attracted to the functional groups. Corry found that a high concentration of charged groups, such as 8 COO^- groups on a CNT of diameter 1.1 nm, completely blocks the transport of both positive and negative ions.[31] Chen *et al.*[32] used simulations to design an asymmetric tip functionalized CNT membrane for salt rejection. The driving force supplied by hydrophilic−hydrophobic ends in smaller tubes (6,6) and (8,8) induced the transport of water while ions were always blocked. Use of larger diameter nanotubes increased the water permeance over narrow CNTs, although the addition of a large number of functional groups reduced the water flux by about a factor of 5. Simulations by Won *et al.* of nanotubes having charges on the walls of the CNTs indicate that the free energy of both water and ions inside the CNTs are affected by the charges.[33] This is consistent with the idea that charges affect the free energy barrier for water and ions entering nanotubes. Joseph *et al.*[34] used MD simulations to explore the occupancy of ions in narrow CNT channels when partial charges were placed on the rim atoms of the nanotubes and an external field was applied along the nanotube axis. The simulation results showed that

the ion occupancy in a CNT solvated in an electrolyte was very low for neutral nanotubes and increased significantly in the presence of charged functionalities. Suk and Aluru[35] have shown that the application of electric fields to nanotubes affects the flux of water under applied pressure for (6,6) CNTs. Therefore, charged groups at the ends of CNTs, which generate electric fields, will also perturb the flux of water.[36] Simulation studies on (10,10) boron nitride nanotubes *versus* (10,10) CNTs show reversed selectivity of K^+ and Cl^- ions due to different entrance effects that result from the difference in charges at the entrance of the nanotubes.[37] Huges *et al.* studied the effect of tip functionalization on water flow through narrow (6,6) and (8,8) CNTs.[38] They compared water diffusion as a function of tip functionalization using hydrogen, hydroxyl, carboxylic acid, and carboxylate functional groups. They found that polar functional groups act to slow water diffusion.[38] These experimental and simulation studies clearly demonstrate the possibility of tuning ion and water transport through functionalizing the entrance of CNTs.

We note in passing that nanoporous graphene is a system that is similar to CNTs; both are one-atom thick materials composed of carbon. Atomistic simulations have been used to predict that porous graphene could also be used for desalination by tuning the size of the pores.[39,40]

Our hypothesis is that CNTs functionalized with chain-like zwitterion groups will be more effective at rejecting both positive and negative ions than CNTs having singly charged functional groups. We postulate that this enhanced performance will be due to a combination of Donnan-type rejection and steric hindrance, because the zwitterion groups are larger and have more conformational degrees of freedom than the functional groups considered in previous simulations.[31] Moreover, zwitterionic groups should prevent biofouling, which is a major problem with current desalination membranes, since zwitterion-treated surfaces have been shown to be resistant to both cell adhesion and biofouling.[41−43] It has been shown that an electrically conductive polymer-nanocomposite membrane containing carbon nanotubes is highly resistant to biofilm formation when an electrical potential is applied across the membrane.[44] We propose that zwitterion functionalized nanotubes could function in a similar way, but without the need for the imposed electrical potential, because the groups have permanent charges. In this study we examine the transport of water and ions through zwitterion-functionalized CNT membranes using both atomically detailed modeling and experimental techniques. We have used zwitterion groups having the following structure: $-COO\text{-}(CH_2)_3\text{-}N^+(CH_3)_2\text{-}(CH_2)_2COO^-$. We have used nonequilibrium MD simulations to calculate both water and ion transport through idealized membranes and have found that addition of two zwitterions per tube end can completely block ion transport in membranes having CNTs with diameters of 15.6 Å. We have synthesized CNT/polyamide nanocomposite membranes using a procedure that partially aligns the CNTs within the polyamide layer through flow filtration.[7] We have measured the performance of the membranes as a function of the concentration of the CNTs. We find that increasing the weight fraction of CNTs leads to an increase of both water transport and ion rejection, indicating that the zwitterion functionalized CNTs are effective at both conducting water and blocking ion transport. Analysis of our simulations shows that the zwitterion moieties lead to the rejection of ionic species *via* a gatekeeper mechanism, involving both steric effects and charge repulsion. Since resistance to water transport is only at the entrance, this provides a distinct advantage over polymer membranes, which have high tortuosity and resistance to water flow throughout the entire thickness of the membrane. Importantly, the synthesis method we have developed can be used for large-scale manufacture of CNT membranes, in contrast to previous CNT membrane synthesis methods,[5,26] which require CNTs to be grown on a substrate. It is this substrate growth that is not scalable.

RESULTS AND DISCUSSION

Water Flux and Ion Rejection. Molecular simulations clearly show that zwitterion functionalized CNTs reject ions, while allowing an acceptable flux of water. A typical simulation cell for single-walled CNT membranes was shown in Figure 1. Each end of each tube was functionalized with 0, 1, or 2 zwitterion groups. The diameter of each tube is about 15 Å, which is similar to the average diameter of CNT using in experiment. The conductance of water and ions for NaCl solutions was calculated at a pressure drop of 208 MPa through pristine and functionalized CNTs. We used this large pressure drop in order to improve the sampling statistics in the simulations, because the time scales accessible in simulations were only on the order of tens of nanoseconds. We note that extrapolation to lower pressure drops can be made since the flux of water has been shown to be a linear function of the pressure drop for both nanotubes[21] and for graphene nanopores.[40] The conductance of water and ions through (20,0) CNTs as a function of simulation time is shown in Figure 2, where the linear increase in conductance with time indicates that the simulations are at steady state. We note from Figure 2 that as the number of zwitterion functional groups per tube increases, the conductance of both water and ions decreases. When each tube end was functionalized with two zwitterions, the conductance of ions decreased to zero while the flow rate of water was reduced, although its magnitude was still significant—about 100 water molecules per

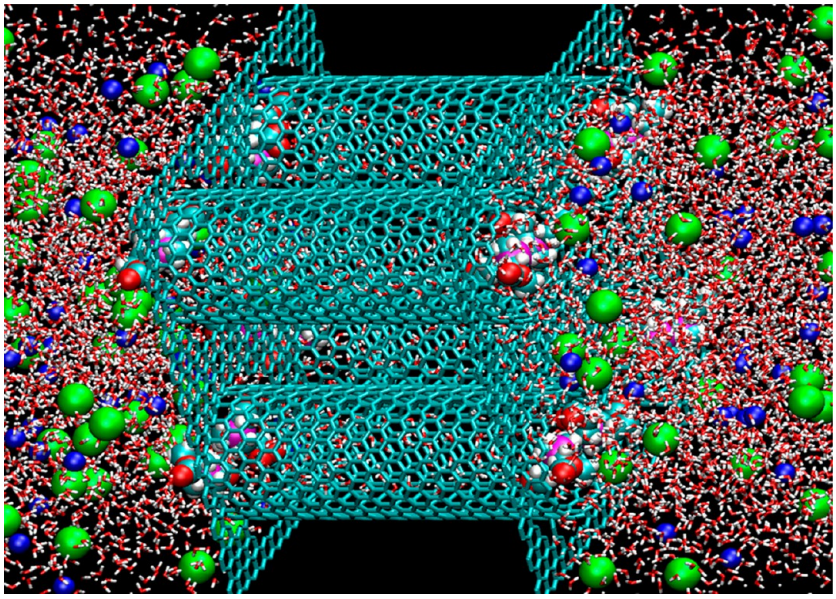

Figure 1. View of the section for simulation cell containing a membrane composed of four CNTs embedded between two graphene sheets with saltwater on either side of the membrane. Each end of each tube is functionalized with two zwitterionic groups. The carbons of the CNTs and graphene sheets are shown as cyan lines. Water molecules are shown as red and white sticks, Cl^- and Na^+ ions are shown as green and blue spheres, respectively, and the atoms of the zwitterions are shown as space filling models, cyan for C, red for O, white for H, and magenta for N.

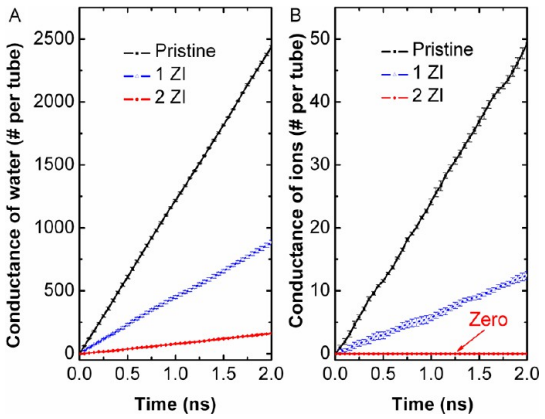

Figure 2. Conductance of (A) water and (B) ions per CNT (20,0) for pristine (nonfunctionalized) nanotubes (black line with solid square), CNTs with one zwitterion (1 ZI) at each end (blue line with empty triangle), and with two zwitterions (2 ZI) at each end (red line with solid circle) for a bulk concentration of 0.6 M NaCl and a pressure drop of 208 MPa. Error bars show the standard deviation based on four independent simulations.

tube per nanosecond. The calculated ion rejection ratio was 100% for the system with two zwitterions per tube end; no ions passed through the CNTs over a total simulation time of 8 ns. The (20,0) CNTs with a single zwitterion on each end has an ion rejection ratio of about 25% and a water flow rate of about 450 H_2O per nanotube per ns. We have also simulated (20,0) CNTs with various numbers of carboxylic acid groups on each end. We found that when five COOH groups are placed at each end that the water and ion flow rates are about the same as for the CNT with a single zwitterion on each end, with a water flow rate of 470 per tube per ns and an ion rejection ratio of about 20%. We note that the water flow rate is higher and the ion rejection ratio is lower for our simulations compared with those for a similar system reported by Corry.[31] This is because a smaller diameter CNT was studied in that work, namely the (8,8) CNT with a diameter of 1.1 nm. We have carried out simulations with 0.6 M KCl for the zwitterion functionalized CNTs and have found results very similar to those for NaCl (Figure S1 of the Supporting Information).

The diameter distribution of CNTs used in experiments ranges from 10 to 20 Å, with an average diameter of 15 Å.[45] One or two zwitterions groups should be adequate to block all ion transport in CNTs having diameters less than 15 Å (*vide supra*). However, we do not know if ion transport can be blocked by the addition of zwitterions for the largest CNTs in the experimental sample. We have therefore simulated a membrane composed (26,0) CNTs, which have a diameter of 20.3 Å. We placed two, four, and five zwitterion groups at the ends of each of the nanotubes in order to determine if zwitterions can completely block ion transport in these large diameter CNTs. As shown in Figure 3, the conductance of water and ions for NaCl solutions was calculated at a pressure drop of 208 MPa through functionalized CNTs. The concentration of saltwater is 0.6 M. The conductance of water and ions decreased as the number of zwitterion groups was increased, as was the case with the (20,0) CNT membrane. When each tube end was functionalized with five zwitterion groups, the ion rejection ratio reached 100%; no ions passed through over a total simulation time of 8 ns. Thus, our simulations predict that even

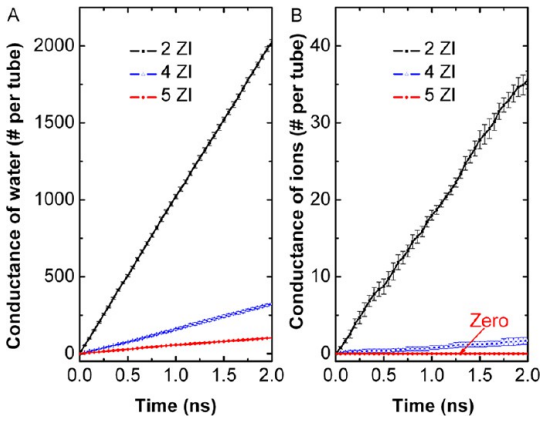

Figure 3. Conductance of (A) water and (B) ions per CNT (26,0) for CNTs with two zwitterions (2 ZI) at each end (black line with solid square), with four zwitterions (4 ZI) at each end (blue line with empty triangle), and with five zwitterions (5 ZI) at each end (red line with solid circle) for a bulk concentration of 0.6 M NaCl at a pressure drop of 208 MPa. Error bars show the standard deviation based on four independent simulations.

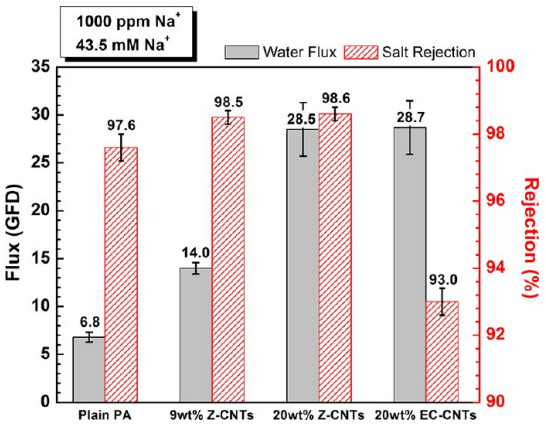

Figure 4. Water flux (solid) and salt rejection ratio (hatched) as a function of CNT concentration in the selective PA layer of the nanocomposite membrane. The concentrations of zwitterions functionalized CNTs (Z-CNTs) are 0 wt % (0 mg), 9 wt % (0.25 mg) and 20 wt % (0.75 mg), respectively. The concentration of end-capped CNTs (EC−CNTs) is 20 wt %. The concentration of Na^+ is 1000 ppm (43.5 mM NaCl). Pressure of 530 psi was applied for each membrane test. Error bars were computed from the standard deviations of the fluxes over a three day period. See Figure S2 in the Supporting Information.

relatively large 20 Å diameter CNTs can have very high rejection ratios if functionalized with a fairly small number of zwitterions.

Three polyamide (PA) membranes were fabricated with 0 (0 wt %), 0.25 (9 wt %) and 0.75 (20 wt %) mg of zwitterion functionalized CNTs deposited in a plain PA matrix with total area of 17.35 cm^2. As a control, a fourth nanocomposite membrane containing 20 wt % end-capped CNTs was also fabricated. The area of each PA membrane that contained the CNTs was 10.75 cm^2 and was located in the center of the PA membrane. The weight percentage reflects the percentage of CNTs in the selective PA layer. These membranes were tested for water and ion flux by using a pressure drop of 3.65 MPa (530 psi) with a feed solution containing 1000 ppm of Na^+ (or ~2500 ppm NaCl or 43.5 mM) The transport results are shown in Figure 4. Adding 0.25 mg CNTs to the PA membrane resulted in the water flux increasing more than 2-fold, from 6.8 GFD (gallons per square foot per day) to 14.0 GFD, while the rejection of Na^+ increased by approximately 1% from 97.6% to 98.5%. Increasing the amount of CNTs to 0.75 mg, the water flux increased by about a factor of 4 (to 28.7 GFD) over the plain PA membrane and the ion rejection ratio remained about constant at 98.6%. Figure 4 also shows that a significant increase in flux was achieved when 20 wt % closed-ended carbon nanotubes were incorporated into the polyamide matrix. However, this increase in water flux was accompanied by a significant drop in salt rejection down to 93%, which is lower than the salt rejection of the neat polyamide membrane.

Each membrane was tested for three consecutive days to examine the membrane stability. All membranes showed stable performance with <1% variability over three days (see Figure S2 in the Supporting Information). We note that commercial PA membranes have significantly better performance than our membranes due to differences in the synthetic procedure.[46] Our purpose at this time is not to produce an optimized PA membrane, but rather show that PA membranes can be significantly improved by the addition of functionalized CNTs. Because there is no trade-off between selectivity and permeability, the experimental results suggest that the functionalized CNTs impart an additional transport mechanism to the membrane. We hypothesize that this mechanism consists of fast fluid flow through the functionalized CNTs, whose zwitterionic groups block the entry of ionic species into the CNT pores, thereby enhancing (or at least preserving) the salt rejection. These results are entirely consistent with the simulation results for the idealized CNT membranes. Increasing the concentration of CNTs provided more channels for the transport of water through the PA membrane, while ions were still blocked due to the zwitterionic groups attached at tube ends. We note that the CNTs are entirely embedded within the PA membrane and are not completely aligned within the PA. This means that there is considerable room for improvement in the synthesis of the composite membrane. An ideal membrane would have CNTs perfectly aligned with the direction of fluid flow and would percolate completely through the membrane, so that no fluid would have to permeate through the polymer. Our membranes are far from optimal by this measure, but they do provide a proof of concept that functionalized CNTs can enhance both water flux and salt rejection.

The fact that the water flux of the end-capped CNT composite membrane also increases significantly in

comparison to the neat polyamide membrane suggests the formation of nanoscaled voids at the interface between the carbon nanotubes and the polymer matrix, at least for the pristine CNTs. These nanochannels allow water and salt ion molecules to travel through the membrane close to the external surface of the CNTs at faster rates than across the polyamide thin layer, leading to a higher water flux but lower selectivity for water/salt ion. It is possible that these nanochannels also exist in the case of the zwitterion-functionalized CNT composite membranes. Since the zwitterionic functional groups are attached not only at the pore entrance of the carbon nanotubes, but also along the wall of SWNTs, they can reject salt ions by size exclusion and Donnan exclusion at the entrance as well as inside the nanochannels. Therefore, it is possible that water molecules travel both inside the SWNTs and around them in the nanochannels. In the case of functionalized carbon nanotubes, both of the paths could be blocked by the zwitterionic groups, which offer good water/ions selectivity. An alternate scenario is that the end-capped CNTs induce voids in the PA membrane while the zwitterion-functionalized CNTs do not. This is based on the following differences between the end-capped and zwitterion-functionalized CNTs: (1) The end-capped CNTs are about a factor of 5 longer than the zwitterion-functionalized tubes, the former being as long as 5 μm, while the latter are about 1 μm in length.[45] It is reasonable to assume that these very long CNTs will disrupt the PA membrane structure to a much larger degree than the shorter CNTs. (2) The end-capped CNTs likely have pristine surfaces with very few functional groups covalently bound to them. In contrast, we estimate that each zwitterion functionalized CNT will have about 6.4×10^3 zwitterions or an average of about one zwitterion for every 30 carbon atoms on the CNT (see Supporting Information). This means that most of the zwitterions will be bound to and distributed along the sidewalls of the CNTs because the ends can only accommodate a small number of functional groups. For example, a (20,0) CNT could have a maximum of 20 zwitterions on each end. Hence, the interfacial surface energies of the end-capped and zwitterion-functionalized CNTs will be very different. We assume that the zwitterions will impart a greater degree of compatibility with the PA, hence, there may not be voids around the zwitterion-functionalized CNTs. This hypothesis is consistent with experiments showing that the pristine end-capped CNTs required the addition of surfactant to be dispersed in the PA, while the zwitterion functionalized CNTs were dispersible in the absence of surfactant (see Materials and Methods section).

It is reasonable to assume that the reduction in water and ion flux in the functionalized nanotubes, shown in Figure 2, is due to a combination of both the steric and electrostatic effects when adding additional

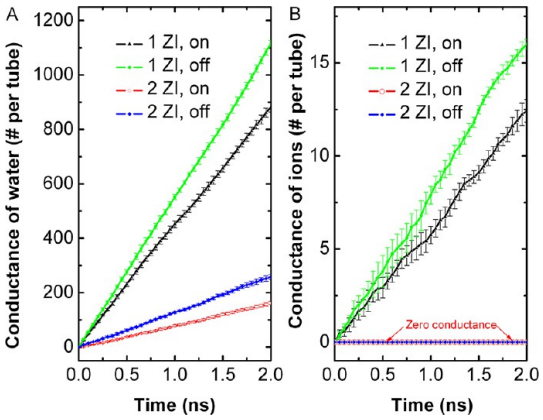

Figure 5. Conductance of (A) water and (B) ions through CNTs functionalized with one or two zwitterions per tube end and with charges on the zwitterions turned on or off. The diameter of each tube is 15.6 Å, corresponding to CNT (20,0). The pressure drop was 208 MPa in each case. Error bars show the standard deviation based on four independent simulations.

zwitterions. To quantify the relative importance of electrostatic and steric effects, we carried out simulations with the partial charges of the zwitterion groups turned off—something that is impossible to do in an experiment. As shown in Figure 5, the conductance of both water and ions increased by about 30% in the 1 zwitterion system when the charges were turned off. In the 2 zwitterion system the ion rejection remained at 100% when the zwitterions charges were turned off, whereas the water conductance increased by about 35%, which is a modest increase given that the drop in water flux from unfunctionalized to functionalized with 2 zwitterions is about 1 order of magnitude. This indicates that steric hindrance is the dominant mechanism for reducing the ion and water flux. The simulations for uncharged groups predict that hydrocarbon functional groups could block ion transport as well. However, the zwitterions impart compatibility with the PA polymer that may be missing in the hydrocarbon functional groups. Moreover, uncharged groups would not show any resistance to biofouling. A similar gating of CNTs was reported by Majumder based on experimental work on multiwalled nanotubes having much larger diameters that were functionalized with charged molecular tethers.[27]

We have used molecular simulations to probe the details of the steric hindrance due to the zwitterions. Unlike short functional groups, such as carboxyalic acids, the zwitterions used in our experiments and simulations are very flexible and can adopt a large number of different conformations. This flexibility is manifested in the simulations by noting that zwitterions, which are initially placed into the solution with their molecular chains in an extended (unfolded) configuration away from the tube pores, tend to fold during the course of the simulation so that they are at least partially folded inside the tube. The configuration

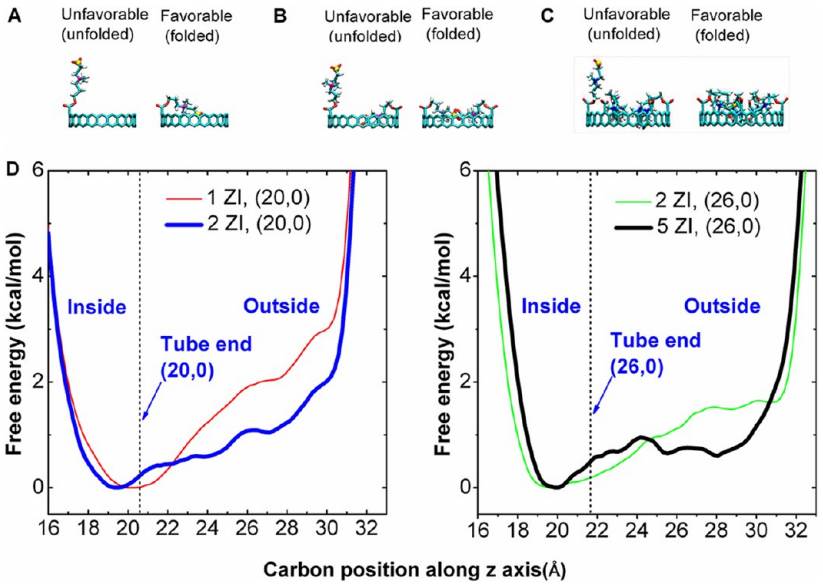

Figure 6. Configurations of zwitterions that are extended (unfolded) into the liquid phase or folded inside the CNT for the (20,0) system with (A) one (1 ZI) or (B) two zwitterions (2 ZI) per tube end and for the (26,0) system with (C) five zwitterions (5 ZI) per tube end. (D) The PMF for moving one zwitterion group from inside (folded) to outside (unfolded) of the CNT, as measured by the terminal carbon atom position on the zwitterion. Left panel: PMF for moving one zwitterion in a (20,0) CNT having one (red) or two (blue) zwitterions per tube end. Right panel: PMF for moving one zwitterion in a (26,0) CNT having two (green) or five (black) zwitterions per tube end. The carbons on the CNT and zwitterion groups are shown as cyan. Oxygen, nitrogen, and hydrogen are shown as red, purple, and white, respectively. The terminal carbon on the zwitterion, shown in yellow (in panels A–C), was constrained in the umbrella sampling simulations. The tube end positions are represented as vertical dash lines in D.

of the zwitterion has a profound effect on the flux of water and ions. When the zwitterion is extended into the solution phase, transport of both ions and water occurs with much less resistance than when the zwitterions are folded into the tube. Steric effects dominate the transport of water and ions in this latter case. It is therefore very important to identify the free energy of the various configurations of the zwitterions. We have computed the potential of mean force (PMF) for the change of free energy for a zwitterion functional group as it moves from a configuration where it is folded inside the nanotube (folded) and to a configuration where it is extended outside the nanotube into the solution phase (unfolded), as shown in Figure 6. We have studied a system composed of (20,0) CNTs functionalized with one or two zwitterions per nanotube end and a system composed of (26,0) CNTs functionalized with two or five zwitterions per tube end. The PMF curves are plotted in Figure 6. It can be seen from Figure 6 that the free energy favors the folded configurations for all systems studied. The zwitterions tend to block tube entrances to reduce the effective pore size when they are folded inside the tubes; this is consistent with our observations in Figure 5 that steric effects dominate over electrostatics. In the system with the (20,0) CNT (left panel in Figure 6D), we estimate that the folded configuration is about 2.9 kcal/mol more favorable than the unfolded configuration for a single zwitterion, and about 2.3 kcal/mol more favorable for having the second zwitterion folded inside the CNT when there are two zwitterions per tube end. The folded configuration is about 1.6 kcal/mol more favorable than the unfolded configuration for the (26,0) CNT system with two zwitterions (right panel in Figure 6D). When there are five zwitterions per tube end, the folded configuration is about 0.5 kcal/mol more favorable than the unfolded configuration, given that the other four zwitterions folded inside the CNT. Given that it is unexpected that all five zwitterions would adopt folded configurations we carried out two more calculations to verify our PMF results. We computed the PMF for moving all five zwitterions from folded to unfolded configurations simultaneously (Figure S3) and found that the free energy favors all five zwitterions being in the folded configuration by about 2.5 kcal/mol, which is, perhaps fortuitously, five times the energy of folding the fifth zwitterion into the tube with the other four already in the folded configuration (right panel in Figure 6D). We also verified that the zwitterions will spontaneously adopt folded configurations by performing MD simulations for a membrane of (26,0) CNTs functionalized with five zwitterions per tube end in a solution of 0.6 M NaCl at 300 K, starting from a configuration where all the zwitterions are in the extended conformation. The initial and final snapshots are shown in Figure S4 of the Supporting Information. Plots of the terminal carbon atom positions on the zwitterions as a function of time are given in Figure S5. From these plots we see that zwitterions quickly adopt folded configurations within a about 0.1 ns and that the ends continue to evolve to more compact, highly folded states as the simulation continues out to 4 ns.

TABLE 1. Water and Ion Flow Rate (Number per Nanosecond per CNT) and Ion Rejection Ratio as a Function of Salt Concentration for Flow through a (20,0) CNT Having One Zwitterion Functional Group at Each End

concentration	cation conductance	anion conductance	total ion conductance	water conductance	ion rejection ratio (%)
0.6 M NaCl	3.8 ± 0.2	3.6 ± 0.1	7.4 ± 0.2	460.0 ± 10.7	24.7 ± 4.3
0.3 M NaCl	2.1 ± 0.2	1.9 ± 0.2	3.9 ± 0.4	500.3 ± 20.3	27.4 ± 9.2
0.6 M KCl	2.7 ± 0.2	3.0 ± 0.4	5.7 ± 0.6	489.9 ± 6.3	45.3 ± 6.3
0.3 M KCl	1.3 ± 0.1	1.7 ± 0.2	3.0 ± 0.2	520.4 ± 10.1	45.9 ± 5.4

We note that the (20,0) and (26,0) CNTs have slightly different lengths in our simulations, as discussed in the Materials and Methods section.

Salt Concentration Effects. We have studied the effect of salt concentration on the ion rejection ratio from both simulations and experiments. We studied the system with one zwitterion group per tube in simulations because two zwitterions per tube end showed total rejection, dominated by steric effects (Figure 5), and would therefore be less sensitive to changes in ion concentration. We carried out flux simulations for 0.6 and 0.3 M NaCl and KCl solutions (13 800 and 6900 ppm for Na^+, 23 400 and 11700 ppm for K^+), both with a pressure drop of 208 MPa. We ran the simulations for 36 ns in order to gather accurate statistics for the ion rejection ratio as a function of concentration. The results are given in Table 1. The simulations indicate that the salt concentration has no effect on the ion rejection ratio, at least for concentrations in the range 0.3−0.6 M. Simulations at much lower concentrations, as those used in experiments, were not feasible because of the low flux of ions and resulting poor statistics.

The concentration of Na^+ in experiments was varied between 50 and 2000 ppm (2.2−43.5 mM) to test for ion concentration effects. We performed experiments with both the plain PA membrane (no CNTs) and the nanocomposite membrane with 20 wt % CNTs in order to test for differences in concentration dependence inherent in the PA membrane as opposed to the functionalized CNTs. The results of these experiments, plotted in Figure 7, show an increase in the salt rejection ratio with ion concentration for both the plain PA membrane and the nanocomposite membrane with 20 wt % CNTs.

The increase in rejection ratio with increasing ion concentration is an unexpected result; indeed, the opposite effect was observed by Fornasiero *et al.*,[30] who found that the ion rejection ratio decreased with increasing ion concentration in the feed, and dropped to zero when the ion concentration was equal to 10 mM for KCl. The difference in the performance between their membranes and ours is due to the mode of ion rejection. Fornasiero *et al.* used negatively charged CNTs membranes, which rejected ions in accordance with the Donnan equilibrium theory.[30] Many nanofiltration membranes are negatively charged and

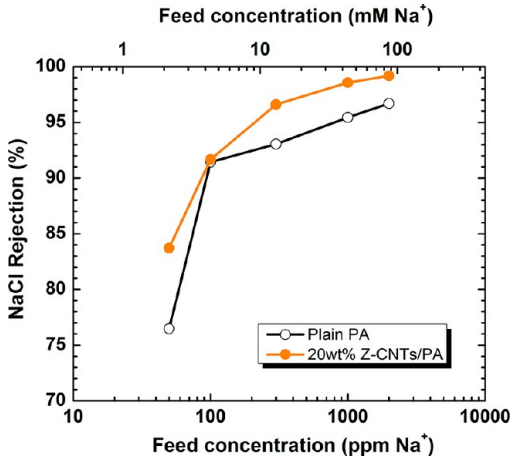

Figure 7. Salt rejection as a function of Na^+ feed concentration for a plain PA membrane (black curve with open circles) and a nanocomposite membrane with 20 wt % CNTs (orange curve with solid circles). Feed pressure of 530 psi.

exhibit electrostatic screening effects.[47−49] Therefore, ion rejection is sensitive to salt concentrations in charged membranes. In contrast, Ji *et al.*[50] showed that addition of zwitterionic groups counteracts the effects of ion concentration. They demonstrated that the ion rejection ratio decreased from 96.5 to 65% as salt concentration was increased from 100 to 3500 ppm $MgCl_2$ for a membrane without zwitterions. However, the addition of zwitterion groups to the membrane gave very stable rejection ratios that were independent of salt concentration.[50] Note that our plain PA membrane, which is uncharged, exhibits an increase in the rejection ratio with increasing concentration of NaCl (over a narrow range of concentrations). This same trend has been observed for other PA-type membranes.[51,52] We therefore attribute the increase in rejection ratio with increasing NaCl concentration observed for the nanocomposite membrane in Figure 7 to the PA component rather than the zwitterion functionalized CNTs. This agrees with our molecular simulations, showing no effect of concentration on the rejection ratio (Table 1).

CONCLUSIONS

We have shown that zwitterion functionalized CNTs can be embedded in a PA membrane and that the performance of the composite membrane increases as the fraction of CNTs is increased. The water flux increases significantly and the ion rejection ratio

increases or remains about the same, indicating that the increased water flux is not due to an increase in nonspecific pores in the membrane, but rather due to an additional transport mechanism resulting from the presence of the functionalized CNTs. Molecular simulations show that the addition of only two zwitterions per nanotube end results in complete rejection of ions, while allowing significant water flux for nanotubes with diameters the same as those used in the experiments. We demonstrate that the ion rejection occurs because of gated entrance into the nanotubes due mainly to steric hindrance of the zwitterions, which adopt thermodynamically favored configurations so that they are folded into the tube end. Finally, we can compute the upper bound of membrane performance based on our simulation results for zwitterion functionalized nanotube. Assuming a membrane containing 20 wt % CNTs, having lengths of 1 μm, and assuming all CNTs are perfectly aligned (which is not the case in our experiments), we estimate a flux of 20 000 GFD for a membrane with a pressure drop of 530 psi (see Supporting Information). This is 3 orders of magnitude greater than our experimentally observed flow rate of 28.7 GFD, indicating that there is ample opportunity to optimize this first-generation membrane.

MATERIALS AND METHODS

Modeling. Molecular dynamics simulations were performed for hypothetical single-walled CNT membranes shown in Figure 1. Two different membranes were considered, one composed of (20,0) CNTs and the other composed of (26,0) CNTs. The diameters of the CNTs were 15.6 and 20.3 Å, respectively. The length of the (20,0) CNTs was 41.18 Å, while the length of the (26,0) CNTs was 43.31 Å. The tubes had different lengths because we inadvertently added a half of a unit cell to the (26,0) CNTs when constructing the tubes. This slight difference in length will not have any effect on the properties. The ends each tube were functionalized with 0, 1, or 2 zwitterionic groups for the (20,0) system and 2, 4, or 5 zwitterions for the (26,0) system. The CNTs were embedded in two graphene sheets to form a membrane. The membrane was immersed into a water box containing NaCl or KCl with periodic boundary conditions along three dimensions. The sizes of the simulation boxes were 54.1 Å × 55.38 Å × 114 Å for the (20,0) CNTs and 68.9 Å × 68.2 Å × 95.3 Å for the (26,0) system. The nominal concentration of salt in seawater of 0.6 M was used for most of the calculations. Selected calculations were also performed for a concentration of 0.3 M. The pressure of the bulk solution was equilibrated to 1 bar. Parameters for carbon atoms in CNTs and graphene sheets were taken as the parameters for aromatic carbon `CA' in the CHARMM27 force field.[53,54] All of the carbon atoms in CNTs and graphene sheets were fixed in place during the dynamic simulation. It has been shown that the flexibility of CNTs only affects the kinetics of transport into a CNT when the pore entrance is about the same size as the molecule.[55] In our case the diameter of the CNTs is much larger than the size of the molecules and the gating effect is controlled by the zwitterion functional groups, which are fully flexible. Water molecules were simulated using the TIP3P water model.[56] The potential parameters for the zwitterion groups were also taken from the CHARMM27 force field,[53,54] except for the atomic charges. The charges on the atoms of the zwitterions were obtained from an electrostatic potential fitting algorithm developed for periodic systems.[57] Details of the procedure are given in the Supporting Information. The parameters for Na^+, K^+ and Cl^- were taken from the literature.[58,59] The temperature of the system was controlled by a Nosé-Hoover thermostat with a damping parameter equal to 100. All calculations were performed with the LAMMPS package[60] using a time step of 1 fs. In the flux calculation, a pressure drop was introduced to generate the flux through the membrane using the method developed by Zhu *et al.*[61] Following the approach of Corry,[21,31] a constant force was applied to each water molecule in the force region of the saltwater box from 45 to 69 Å in the (20,0) system and from 40 to 55 Å in the (26,0) system.

Potential of mean force calculations for the zwitterion end group moving from inside to outside the nanotube were computed using the umbrella sampling method[62] in conjunction with weighted histogram analysis method (WHAM) using Grossfeld's code.[63] A one-dimensional spring potential, $U = k_z(z - z_0)^2$, was applied along tube axis direction to each sampled zwitterion group. The spring force constant k_z was equal to 1 kcal/(mol/Å^2). The sampling region from z = 15.5 Å to z = 35 Å was divided into 40 windows; the size of each window was equal to 0.5 Å. In the system with two zwitterions, another spring, $U' = k_z'(z - z_0')^2$, was applied to the unsampled zwitterion groups with z_0' = 20.5 Å. This guaranteed that the second zwitterion group (unsampled zwitterion) remained around the tube end during the sampling for the first zwitterion group. The spring force constant k_z' was equal to 1 kcal/(mol/Å^2). In the system with five zwitterion groups at each tube end, a larger spring force constant k_z = 3 kcal/(mol/Å^2) was applied in order to improve sampling. The sampling time for each window was 500 ps with the first 100 ps discarded for equilibration. We have checked the convergence of the PMF calculations by comparing PMF taking sampling times of 200, 300, or 400 ps for each window. Results from these shorter sampling times are in good quantitative agreement with the 400 ps sampling. Details of the WHAM method are given in the Supporting Information.

The ion rejection ratio was calculated from simulations using the definition

$$R(\%) = \left(1 - \frac{J_{ion}}{J_{water}} \times \frac{C_{water}}{C_{ion}}\right) \times 100 \qquad (1)$$

where J_{ion} and J_{water} are the conductance of ions and water, respectively, and C_{ion} and C_{water} are the concentrations of ions and water in the bulk phase, respectively. The concentrations of the bulk phase were taken to be constant and the flux was estimated by computing the ensemble average of the conductance of ions and water through the CNTs on a per-nanotube basis. Error bars were computed from the estimated sample standard deviations of the conductance, based on block averages.

Materials. The following chemicals were purchased from Sigma-Aldrich: 1,3,5-benzenetricarbonyl trichloride (trimesoyl chloride, TMC), 1,3-phenylenediamine (*m*-phenylenediamine, MPD) and sodium dodecylbenzenesulfonate (SDBS) were used as received. All chemical were of analytical grade. Polyethersulfone (PES) ultrafiltration membranes were provided by Trisep Corporation (Goleta, CA).

CNT Functionalization. Carboxylate functionalized CNTs of outer diameter 15 Å and length 1 μm were purchased from Nano Lab Inc. (Waltham, MA).[45] The COOH− functionalized CNTs were produced by chemical vapor deposition (CVD). Concentration of −COOH groups in the CNTs was approximately 2−7 wt % (as determined by titration). The functionalized CNTs were reacted with thionyl chloride ($SOCl_2$) at 65 °C for 36 h and the −COOH groups were replaced by COCl groups. The acylated CNTs were then esterificated using 3-dimethylamino-1-propanol, $(CH_3)_2$-N-C_3H_6-OH. This was followed by a ring-opening reaction of lactone, in which β-propiolactone was opened to form an acid group and attached to the tertiary amine on the functional group.[64,65] The resulting zwitterionic group had a positive charge at the tertiary amine group and negative charge at the carboxylated group.

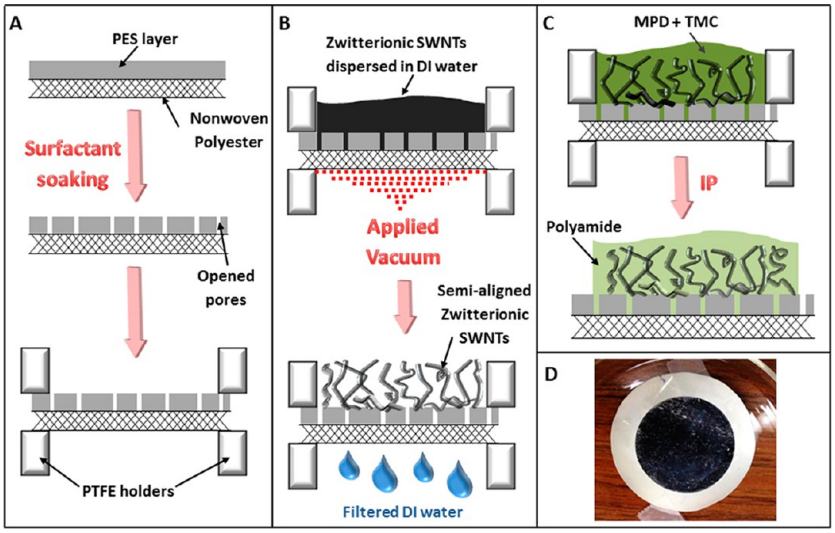

Figure 8. Cross-sectional schematics of the fabrication procedure for CNT nanocomposite membrane. (A) PES ultrafiltration membrane, composed of a thin PES layer covered on a nonwoven polyester web, soaked in surfactant solution to clean the pores and increase hydrophilicity. The membrane was then sandwiched by two PTFE holders. (B) Zwitterion functionalized CNTs, depositing onto the pretreated PES membrane, through vacuum filtration. (C) Interfacial polymerization of polyamide carried out between semialigned functionalized CNTs at which aqueous solution of MPD comes in contact with nonaqueous solution of TMC. (D) Photograph of the top of CNT nanocomposite membrane that is exposed to the feed.

Membrane Fabrication. *Functionalized CNT Nanocomposite Membranes.* Briefly, the fabrication process was divided into three steps, as shown schematically in Figure 8. First, the PES support was pretreated by soaking in 0.5 wt % SDBS solution to open the pores and to increase the hydrophilicity. Field emission scanning electron microscopy (FESEM) was used to examine the surface of the support, as shown in Figure S6A and described in the Supporting Information. The support was sandwiched between two round poly(tetrafluoroethylene) (PTFE) holders. Afterward, a predetermined amount of functionalized CNTs was poured on the support. We used high-vacuum filtration to disperse the CNTs on the support in a semialigned orientation[7] and to remove the solvent. The third step in the membrane fabrication process was interfacial polymerization of PA. In this step, the support with semialigned CNTs was wetted in turn with 2 wt % MPD (with 0.2 wt % of SDBS) and 0.5% (w/v) TMC solutions before polymerization. The PA apparently completely covers the CNTs, as can be inferred by comparing the FESEM images for the plane PA and the CNT/PA membrane surfaces in Figure S3B,C. The partial alignment of the CNTs within the PA layer can be observed from the FESEM image of the cross section of the CNT/PA membrane shown in Figure S6D. Details of the fabrication procedure are given in the Supporting Information.

End-Capped CNT Nanocomposite Membranes. The end-capped SWNTs were purchased from NanoLab, Inc.[45] and used as received without any further purification. They were produced by CVD method, with diameter of 15 Å and length of 1 to 5 μm. Unlike the zwitterionic functionalized SWNTs, end-capped SWNTs required the presence of surfactant in the solution to maintain a well-dispersed phase. In this case, 10 mg of SBDS was added into 40 mL of deionized water to create a 0.025 wt % SBDS solution. A certain amount of end-capped SWNTs, depending on the desired concentration of SWNTs in the membrane, was then dispersed in the SBDS solution by sonication. Using the identical fabrication method outline above, end-capped SWNTs were deposited and semialigned on a pretreated membrane support by filtration, followed with an interfacial polymerization of the polyamide carried out on the CNTs-attached support. After 5 min of oven curing, the fresh nanocomposite membrane was washed thoroughly with DI water, submersed in fresh DI water and stored in a laboratory refrigerator at 4 °C.

Membrane Characterization. Pressure-driven experiments were carried out on a laboratory-scale cross-flow membrane test unit, capable of pressures from 25 to 1000 psi. This test unit is comprised of a membrane cell (GE Sepa CF II Cell), high pressure pump (Hydra-cell pump, Warner Engineering), back-pressure regulator (US Paraplate), bypass valve (Swagelock), feedwater reservoir (Nalgene), operated in closed loop mode with retentate being circulated into the feedwater reservoir. The concentration analysis of the sodium cation present in the permeant was measured by a sodium ion-selective electrode (Thermo Scientific; 8611BNWP, MA).

Membrane Permeation Tests. The membrane cell was pressurized to the designated hydraulic pressure by adjusting the speed of the pump and the flow rate of the retentate. For each testing pressure, the permeation flux was allowed to equilibrate for 30 min before any permeant collection. A known amount of permeant was collected in a glass vial within a given period of time. The density of water was taken to be 0.997 g/cm^2 at ambient temperature, the volumetric flow rate was calculated from $Q = (\Delta V/tA)$, where ΔV is the permeate volume (U.S. gallon), t is the permeation time (day) and A is the effective membrane area (ft^2). The flow rate, Q, is in the unit of gallon per square foot per day (GFD).

The sodium ion electrode was calibrated using a standard sodium solution with concentration of 1000 $\pm$ 5 ppm Na^+. The atomic absorption spectrophotometer (AAS) was also calibrated using standard solutions, which contained 5, 10, 15, and 20 ppm of the specific cations, respectively. Thus, the concentrations of cations in the feed, C_f, and the permeant, C_p, were measured and the salt rejection ratio (in percent) was calculated from

$$R(\%) = \left(1 - \frac{C_p}{C_f}\right) \times 100 \qquad (2)$$

Conflict of Interest: The authors declare no competing financial interest.

Acknowledgment. This work was supported by grants from NSF-CBET 0755937 and from the US Bureau of Reclamation R10AP81214. M.G.T. was supported through an NSF REU site grant, EEC-1005048. We thank the Center for Simulation and Modeling for computer time. We thank De-Li Chen and Bo Zhang for helpful discussions.

Supporting Information Available: Details of the membrane fabrication procedures, CNT characterization, the zwitterion charge fitting method, estimation of flux error bars, estimation

of flux through an ideal membrane, estimation of the number of zwitterions per nanotube, details of WHAM calculations, potentials of mean force plots, zwitterion folding simulation plots, and flux experiments over three days. This material is available free of charge *via* the Internet at http://pubs.acs.org.

REFERENCES AND NOTES

1. WHO/UNICEF. Progress on Drinking Water and Sanitation 2012, pp 1−58. http://www.who.int/water_sanitation_health/publications/2012/jmp_report/en/.
2. Gleeson, T.; Wada, Y.; Bierkens, M. F. P.; van Beek, L. P. H. Water Balance of Global Aquifers Revealed by Groundwater Footprint. *Nature* **2012**, *488*, 197−200.
3. Gleick, P. H. Water Resources. In *Encyclopedia of Climate and Weather*; Schneider, S. H., Ed.; Oxford University Press: New York, 1996; Vol. 2, pp 817−823.
4. Al-Ahmad, M.; Aleem, F. A. A.; Mutiri, A.; Ubaisy, A. Biofouling in RO Membrane Systems Part 1: Fundamentals and Control. *Desalination* **2000**, *132*, 173–179.
5. Holt, J. K.; Park, H. G.; Wang, Y.; Stadermann, M.; Artyukhin, A. B.; Grigoropoulos, C. P.; Noy, A.; Bakajin, O. Fast Mass Transport through Sub-2-Nanometer Carbon Nanotubes. *Science* **2006**, *312*, 1034–1037.
6. Kim, S.; Chen, L.; Johnson, J. K.; Marand, E. Polysulfone and Functionalized Carbon Nanotube Mixed Matrix Membranes for Gas Separation: Theory and Experiment. *J. Membr. Sci.* **2007**, *294*, 147–158.
7. Kim, S.; Jinschek, J. R.; Chen, H.; Sholl, D. S.; Marand, E. Scalable Fabrication of Carbon Nanotube/Polymer Nanocomposite Membranes for High Flux Transport. *Nano Lett.* **2007**, *7*, 2806–2811.
8. Majumder, M.; Chopra, N.; Andrews, R.; Hinds, B. J. Nanoscale Hydrodynamics—Enhanced Flow in Carbon Nanotubes. *Nature* **2005**, *438*, 44–44.
9. Majumder, M.; Chopra, N.; Hinds, B. J. Effect of Tip Functionalization on Transport through Vertically Oriented Carbon Nanotube Membranes. *J. Am. Chem. Soc.* **2005**, *127*, 9062–9070.
10. Skoulidas, A. I.; Ackerman, D. M.; Johnson, J. K.; Sholl, D. S. Rapid Transport of Gases in Carbon Nanotubes. *Phys. Rev. Lett.* **2002**, *89*, 185901.
11. Skoulidas, A. I.; Sholl, D. S.; Johnson, J. K. Adsorption and Diffusion of Carbon Dioxide and Nitrogen through Single-Walled Carbon Nanotube Membranes. *J. Chem. Phys.* **2006**, *124*, 054708.
12. Surapathi, A.; Herrera-Alonso, J.; Rabie, F.; Martin, S.; Marand, E. Fabrication and Gas Transport Properties of SWNT/Polyacrylic Nanocomposite Membranes. *J. Membr. Sci.* **2011**, *375*, 150–156.
13. Majumder, M.; Chopra, N.; Hinds, B. J. Mass Transport through Carbon Nanotube Membranes in Three Different Regimes: Ionic Diffusion and Gas and Liquid Flow. *ACS Nano* **2011**, *5*, 3867–3877.
14. Holt, J. K. Carbon Nanotubes and Nanofluidic Transport. *Adv. Mater.* **2009**, *21*, 3542–3550.
15. Holt, J. K.; Koy, A.; Huser, T.; Eaglesham, D.; Bakajin, O. Fabrication of a Carbon Nanotube-Embedded Silicon Nitride Membrane for Studies of Nanometer-Scale Mass Transport. *Nano Lett.* **2004**, *4*, 2245–2250.
16. Skoulidas, A. I.; Sholl, D. S. Transport Diffusivities of CH_4, CF_4, He, Ne, Ar, Xe, and SF_6 in Silicalite from Atomistic Simulations. *J. Phys. Chem. B* **2002**, *106*, 5058–5067.
17. Kalra, A.; Garde, S.; Hummer, G. Osmotic Water Transport through Carbon Nanotube Membranes. *Proc. Natl. Acad. Sci. U.S.A.* **2003**, *100*, 10175–10180.
18. Zhu, F.; Tajkhorshid, E.; Schulten, K. Theory and Simulation of Water Permeation in Aquaporin-1. *Biophys. J.* **2004**, *86*, 50–57.
19. Thomas, J. A.; McGaughey, A. J. H. Water Flow in Carbon Nanotubes: Transition to Subcontinuum Transport. *Phys. Rev. Lett.* **2009**, *102*, 184502–184502.
20. Thomas, J. A.; McGaughey, A. J. H. Reassessing Fast Water Transport through Carbon Nanotubes. *Nano Lett.* **2008**, *8*, 2788–2793.
21. Corry, B. Designing Carbon Nanotube Membranes for Efficient Water Desalination. *J. Phys. Chem. B* **2008**, *112*, 1427–1434.
22. Song, C.; Corry, B. Intrinsic Ion Selectivity of Narrow Hydrophobic Pores. *J. Phys. Chem. B* **2009**, *113*, 7642–7649.
23. Yu, M.; Funke, H. H.; Falconer, J. L.; Noble, R. D. Gated Ion Transport through Dense Carbon Nanotube Membranes. *J. Am. Chem. Soc.* **2010**, *132*, 8285–8290.
24. Sun, L. F.; Xie, S. S.; Liu, W.; Zhou, W. Y.; Liu, Z. Q.; Tang, D. S.; Wang, G.; Qian, L. X. Materials: Creating the Narrowest Carbon Nanotubes. *Nature* **2000**, *403*, 384–384.
25. Cannon, J.; Kim, D.; Maruyama, S.; Shiomi, J. Influence of Ion Size and Charge on Osmosis. *J. Phys. Chem. B* **2012**, *116*, 4206–4211.
26. Hinds, B. J.; Chopra, N.; Rantell, T.; Andrews, R.; Gavalas, V.; Bachas, L. G. Aligned Multiwalled Carbon Nanotube Membranes. *Science* **2004**, *303*, 62–65.
27. Majumder, M.; Zhan, X.; Andrews, R.; Hinds, B. J. Voltage Gated Carbon Nanotube Membranes. *Langmuir* **2007**, *23*, 8624–8631.
28. Majumder, M.; Corry, B. Anomalous Decline of Water Transport in Covalently Modified Carbon Nanotube Membranes. *Chem. Commun.* **2011**, *47*, 7683–7685.
29. Fornasiero, F.; Bin In, J.; Kim, S.; Park, H. G.; Wang, Y.; Grigoropoulos, C. P.; Noy, A.; Bakajin, O. pH-Tunable Ion Selectivity in Carbon Nanotube Pores. *Langmuir* **2010**, *26*, 14848–14853.
30. Fornasiero, F.; Park, H. G.; Holt, J. K.; Stadermann, M.; Grigoropoulos, C. P.; Noy, A.; Bakajin, O. Ion Exclusion by Sub-2-nm Carbon Nanotube Pores. *Proc. Natl. Acad. Sci. U.S.A.* **2008**, *105*, 17250–17255.
31. Corry, B. Water and Ion Transport through Functionalised Carbon Nanotubes: Implications for Desalination Technology. *Energy Environ. Sci.* **2011**, *4*, 751–759.
32. Chen, Q. W.; Meng, L. Y.; Li, Q. K.; Wang, D.; Guo, W.; Shuai, Z. G.; Jiang, L. Water Transport and Purification in Nanochannels Controlled by Asymmetric Wettability. *Small* **2011**, *7*, 2225–2231.
33. Won, C. Y.; Joseph, S.; Aluru, N. R. Effect of Quantum Partial Charges on the Structure and Dynamics of Water in Single-Walled Carbon Nanotubes. *J. Chem. Phys.* **2006**, *125*, 114701–114701.
34. Joseph, S.; Aluru, N. R. Why are Carbon Nanotubes Fast Transporters of Water? *Nano Lett.* **2008**, *8*, 452–458.
35. Suk, M. E.; Aluru, N. R. Effect of Induced Electric Field on Single-File Reverse Osmosis. *Phys. Chem. Chem. Phys.* **2009**, *11*, 8614–8619.
36. Joseph, S.; Mashl, R. J.; Jakobsson, E.; Aluru, N. R. Electrolytic Transport in Modified Carbon Nanotubes. *Nano Lett.* **2003**, *3*, 1399–1403.
37. Won, C. Y.; Aluru, N. R. A Chloride Ion-Selective Boron Nitride Nanotube. *Chem. Phys. Lett.* **2009**, *478*, 185–190.
38. Hughes, Z. E.; Shearer, C. J.; Shapter, J.; Gale, J. D. Simulation of Water Transport Through Functionalized Single-Walled Carbon Nanotubes. *J. Phys. Chem. C* **2012**, *116*, 24943–24953.
39. Sint, K.; Wang, B.; Král, P. Selective Ion Passage through Functionalized Graphene Nanopores. *J. Am. Chem. Soc.* **2008**, *130*, 16448–16449.
40. Cohen-Tanugi, D.; Grossman, J. C. Water Desalination across Nanoporous Graphene. *Nano Lett.* **2012**, *12*, 3602–3608.
41. Cheng, G.; Li, G. Z.; Xue, H.; Chen, S. F.; Bryers, J. D.; Jiang, S. Y. Zwitterionic Carboxybetaine Polymer Surfaces and Their Resistance to Long-Term Biofilm Formation. *Biomaterials* **2009**, *30*, 5234–5240.
42. Ladd, J.; Zhang, Z.; Chen, S.; Hower, J. C.; Jiang, S. Zwitterionic Polymers Exhibiting High Resistance to Nonspecific Protein Adsorption from Human Serum and Plasma. *Biomacromolecules* **2008**, *9*, 1357–1361.
43. Li, G. Z.; Cheng, G.; Xue, H.; Chen, S. F.; Zhang, F. B.; Jiang, S. Y. Ultra Low Fouling Zwitterionic Polymers with a Biomimetic Adhesive Group. *Biomaterials* **2008**, *29*, 4592–4597.

44. de Lannoy, C.-F.; Jassby, D.; Gloe, K.; Gordon, A. D.; Wiesner, M. R. Aquatic Biofouling Prevention by Electrically Charged Nanocomposite Polymer Thin Film Membranes. *Environ. Sci. Technol.* **2013**, *47*, 2760–2768.
45. NanoLab, Inc., 179 Bear Hill Road, Waltham, MA 02451.
46. Xie, W.; Geise, G. M.; Freeman, B. D.; S., L. H.; Byun, G.; Mcgrath, J. E. Polyamide Interfacial Composite Membranes Prepared from m-Phenylene Diamine, Trimesoyl Chloride and a New Disulfonated Diamine. *J. Membr. Sci.* **2012**, *403*−*404*, 152–161.
47. Bellona, C.; Drewes, J. E.; Xu, P.; Amy, G. Factors Affecting the Rejection of Organic Solutes during NF/RO Treatment—A Literature Review. *Water Res.* **2004**, *38*, 2795–2809.
48. Chung, C. V.; Buu, N. Q.; Chau, N. H. Influence of Surface Charge and Solution pH on the Performance Characteristics of a Nanofiltration Membrane. *Sci. Technol. Adv. Mater.* **2005**, *6*, 246–250.
49. Peeters, J. M. M.; Boom, J. P.; Mulder, M. H. V.; Strathmann, H. Retention Measurements of Nanofiltration Membranes with Electrolyte Solutions. *J. Membr. Sci.* **1998**, *145*, 199–209.
50. Ji, Y.-L.; An, Q.-F.; Zhao, Q.; Sun, W.-D.; Lee, K.-R.; Chen, H.-L.; Gao, C.-J. Novel Composite Nanofiltration Membranes Containing Zwitterions with High Permeate Flux and Improved Anti-Fouling Performance. *J. Membr. Sci.* **2012**, *390*, 243–253.
51. Yu, S.; Liu, M.; Lue, Z.; Zhou, Y.; Gao, C. Aromatic-Cycloaliphatic Polyamide Thin-Film Composite Membrane with Improved Chlorine Resistance Prepared from m-Phenylenediamine-4-methyl and Cyclohexane-1,3,5-tricarbonyl Chloride. *J. Membr. Sci.* **2009**, *344*, 155–164.
52. Bandini, S.; Drei, J.; Vezzani, D. The Fole of pH and Concentration on the Ion Rejection in Polyamide Nanofiltration Membranes. *J. Membr. Sci.* **2005**, *264*, 65–74.
53. Feller, S. E.; MacKerell, A. D. An Improved Empirical Potential Energy Function for Molecular Simulations of Phospholipids. *J. Phys. Chem. B* **2000**, *104*, 7510–7515.
54. Klauda, J. B.; Brooks, B. R.; MacKerell, A. D.; Venable, R. M.; Pastor, R. W. An *Ab Initio* Study on the Torsional Surface of Alkanes and its Effect on Molecular Simulations of Alkanes and a DPPC Bilayer. *J. Phys. Chem. B* **2005**, *109*, 5300–5311.
55. Bucior, B. J.; Chen, D.-L.; Liu, J.; Johnson, J. K. Porous Carbon Nanotube Membranes for Separation of H_2/CH_4 and CO_2/CH_4 Mixtures. *J. Phys. Chem. C* **2012**, *116*, 25904–25910.
56. Jorgensen, W. L.; Chandrasekhar, J.; Madura, J. D.; Impey, R. W.; Klein, M. L. Comparison of Simple Potential Functions for Simulating Liquid Water. *J. Chem. Phys.* **1983**, *79*, 926–935.
57. Chen, D. L.; Stern, A. C.; Space, B.; Johnson, J. K. Atomic Charges Derived from Electrostatic Potentials for Molecular and Periodic Systems. *J. Phys. Chem. A* **2010**, *114*, 10225–10233.
58. Wander, M. C. F.; Shuford, K. L. Molecular Dynamics Study of Interfacial Confinement Effects of Aqueous NaCl Brines in Nanoporous Carbon. *J. Phys. Chem. C* **2010**, *114*, 20539–20546.
59. Dzubiella, J.; Hansen, J. P. Electric-Field-Controlled Water and Ion Permeation of a Hydrophobic Nanopore. *J. Chem. Phys.* **2005**, *122*, 234706–14.
60. Plimpton, S. Fast Parallel Algorithms for Short Range Molecular Dynamics. *J. Comput. Phys.* **1995**, *117*, 1–19.
61. Zhu, F. Q.; Tajkhorshid, E.; Schulten, K. Pressure-Induced Water Transport in Membrane Channels Studied by Molecular Dynamics. *Biophys. J.* **2002**, *83*, 154–160.
62. Torrie, G. M.; Valleau, J. P. Monte Carlo Free Energy Estimates Using Non-Boltzmann Sampling: Application to the Sub-Critical Lennard-Jones Fluid. *Chem. Phys. Lett.* **1974**, *28*, 578–581.
63. Grossfield, A. *WHAM: the Weighted Histogram Analysis Method*, version 2.0.6; 2012, http://membrane.urmc.rochester.edu/content/wham.
64. Zhang, Z.; Chen, S.; Jiang, S. Dual-Functional Biomimetic Materials: Nonfouling Poly(carboxybetaine) with Active Functional Groups for Protein Immobilization. *Biomacromolecules* **2006**, *7*, 3311–3315.
65. Surapathi, A.; Chen, H.-y.; Marand, E.; Karl Johnson, J.; Sedlakova, Z. Gas Sorption Properties of Zwitterion-Functionalized Carbon Nanotubes. *J. Membr. Sci.* **2013**, *429*, 88–94.